Carbon ionization states and the cosmic far-UV background with HeII absorption

Evgenii O. Vasiliev

Institute of Physics, Southern Federal University, Stachki Ave. 194, Rostov-on-Don, 344090, Russia

eugstar@mail.ru

Shiv K. Sethi

Raman Research Institute, Sadashiva Nagar, Bangalore 560080, India

sethi@rri.res.in

Biman B. Nath

Raman Research Institute, Sadashiva Nagar, Bangalore 560080, India

biman@rri.res.in

Received _____; accepted _____

ABSTRACT

We constrain the spectrum of the cosmic ultraviolet background radiation by fitting the observed abundance ratios carbon ions at $z \sim 2$–3 with those expected from different models of the background radiation. We use the recently calculated modulation of the background radiation between 3 and 4 Ryd due to resonant line absorption by intergalactic HeII, and determine the ratios of CIII to CIV expected at these redshifts, as functions of metallicity, gas density and temperature. Our analysis of the observed ratios shows that 'delayed reionization' models, which assume a large fraction of HeII at $z \sim 3$, is not favored by data. Our results suggest that HeII reionization was inhomogeneous, consistent with the predictions from recent simulations.

Subject headings: cosmology: theory – diffuse radiation – intergalactic medium – quasars: general

1. Introduction

Cosmological simulations of the intergalactic medium (IGM) have been used in the recent years to determine many important aspects of structure formation and reionization. One important input for these simulations, the cosmic ultraviolet background radiation, however, has remained uncertain. Our knowledge of the cosmic UV background, its intensity and spectrum and evolution with time, still lacks the precision that is needed to make the interpretations from cosmological simulations robust.

It is believed that HeII reionization occurred much after the reionization of HI and HeI, with the help of hard UV photons from quasars, whose activity peaked around redshift $z \sim 3$. This is because of the relatively high ionization threshold of HeII (54.4 eV) (e.g., Madau & Meiksin 1994; Sokasian et al. 2002). Some recent observations may have found evidences for HeII Gunn-Peterson trough in the spectra of quasars at $z \geq 2.8$ (e.g., Jakobsen et al. 1994; Schaye et al. 2000; Smette et al. 2002). Numerical simulations of HeII reionization (McQuinn et al. 2009) also predict that the process is likely to be inhomogeneous, and accompanied by heating of the IGM. There are some evidences for such a heating from recent observations, although the interpretations are not yet clear (e.g., Ricotti et al. 2000; Schaye et al. 2000; Theuns et al. 2002; Bernardi et al. 2003).

Recently, Madau & Haardt (2009) pointed out an important aspect of the evolution of UV background radiation in the context of HeII reionization. They calculated the effect of resonant absorption by HeII Lyman series that is likely to significantly change the shape of the UV background radiation between 3 and 4 Ryd, whose magnitude depends on the abundance of HeII in the IGM. This modulation can be an important probe of the UV background radiation, when combined with the observations of absorption lines from metal ions such as CIII, whose ionization potential lies between energies corresponding to 3 and 4 Ryd.

In this paper, we use the data from Agafonova et al. (2007) of column densities of CIII and CIV in the redshift range of $z \sim 2$–3, to constrain the spectrum of the UV background radiation. Agafonova et al. (2007) used their observations to recover the shape of the spectrum with a Monte Carlo procedure, but their assumption for the shape of the spectrum did not include the possible attenuation between 3 and 4 Ryd. They claimed a sharp reduction in the flux of the UV background between 3 and 4 Ryd, which was interpreted as a sign of HeII Gunn-Peterson (GP) effect. In this regard, it is important to study the ionic ratios, especially those involving CIII, whose ionization potential falls between 3 and 4 Ryd, and the effect of background radiations of different spectrum on these ratios. One of the predictions made by Madau & Haardt (2009) was that the modulation of the spectrum by HeII absorption would significantly change the abundance ratio of CIII/CIV at $z \sim 3$, and a large CIII/CIV ratio could be explained without any need to invoke the HeII GP effect. We test these ideas in this paper.

2. Calculations of ionic states

We study the thermal and ionization evolution of gas exposed to external ionizing radiation. Our calculation of the evolution of gas is similar to Gnat & Sternberg (2007, 2009). A detailed description of thermal and ionization evolution of gas can be found in Vasiliev (2010). Here we briefly describe the method of calculation, present several tests of our code and discuss the choice of initial conditions.

2.1. The description of the code

A gas parcel is assumed to be optically thin for the ionizing radiation. We consider the time-dependent equations for all ionization states of H, He, C, N, O, Ne and Fe,

including all relevant atomic processes. Namely, we take into account the following major processes: photoionization, collisional ionization, radiative and dielectronic recombination as well as charge transfer in collisions with hydrogen and helium atoms and ions. Atomic data for the photoionization cross section are adopted from Verner et al. (1996); Verner & Yakovlev (1995), Auger effect probabilities taken from Kaastra & Mewe (1993), the recombination rate, for radiative recombination taken from Verner & Ferland (1996), Pequignot et al. (1991), Arnaud & Raymond (1992) and Shull & van Steenberg (1982), for dielectronic recombination adopted from Mazzotta et al. (1998), and for the collisional ionization rate adopted from Voronov (1997), for the charge transfer rates of ionization and recombination with hydrogen and helium adopted from Arnaud & Rothenflug (1985) and Kingdon & Ferland (1996).

This system of time-dependent ionization state equations should be complemented by the temperature equation, which accounts for all relevant cooling and heating processes. Here we assume that a gas parcel cools isochorically, i.e. the cooling time is shorter than any dynamical time scale. Note that in the temperature equation we neglect the change in the number of particles in the system (which for a fully ionized plasma of hydrogen and helium remains approximately constant).

The total cooling and heating rates are calculated using the photoionization code CLOUDY (ver. 08.00, Ferland et al. 1998). More specifically, we incorporate into the CLOUDY code a given set of all ionic fractions X_i calculated at temperature T, gas number density n and external ionization flux $J(\nu)$ and obtain the corresponding cooling and heating rates. For the solar metallicity case we adopt the abundances reported by Asplund et al. (2005), except Ne for which the enhanced abundance is adopted (Drake & Testa 2005). In all our calculations we assume the helium mass fraction to be $Y_{\rm He} = 0.24$.

We solve a set of 68 coupled equations (67 for all ionization states of the elements H,

He, C, N, O, Ne and Fe and one for temperature) using a Variable-coefficient Ordinary Differential Equation solver (Brown et al. 1989). The time step is chosen to be the minimum value between $(0.1t_{ion}, 0.01t_{cool})$, where t_{ion} and t_{cool} are the ionization and cooling times correspondingly.

We study the ionization and thermal evolution of a lagrangian element of cooling gas exposed to extragalactic spectra calculated by using the radiative transfer in the cosmological simulations (Madau & Haardt 2009) with and without the absorption in the He II resonant lines. Figure 1 shows the extragalactic spectra used here. A brief description of the spectra is presented in Section 3. In our simulations we take into account the radiation spectrum from 1 to 10^4 eV.

The evolution of the gas certainly depends on a choice of the initial condition of gas, namely, the initial ionic composition and temperature. We consider such a dependence below (section 2.3). But first, we present several tests of the method of calculation. In these tests we start our calculations from temperature $T = 10^8$ K with the collisional equilibrium ion abundances. During the calculation the gas number density is assumed to remain unchanged due to any dynamical or chemical processes. We stop our calculations when photoionization heating rate differs from cooling rate by less than 5% ($|\Gamma - \Lambda|/\Lambda < 0.05$). The ionic composition is almost "frozen" at this moment. Note that with such a stopping criterion a gas still remains "time-dependent" at the end of the computation, as it has not yet reached thermal and ionization equilibrium.

2.2. Tests of the code

Figures 2-3 present the main tests of our code used in the calculations at the temperature range interested in this paper. Figure 2 shows the carbon ionization fractions

I-IV in the collisional equilibrium obtained from our code (crosses of various types) and original results by Mazzotta et al. (1998) as well as the standard CIE test of the CLOUDY code. One can see a good coincidence between the results of our code and those obtained in the previous works.

We show the comparison between the cases of photoionization equilibrium and time-dependent photoionization as well as collisional time-dependent and equilibrium with regard to CIII fraction in Figure 3. The case of photoionization equilibrium is shown with thick dash-dot lines and that of the time-dependent photoionization is shown by thick dot lines. We use a density of $n = 10^{-4}\mathrm{cm}^{-3}$ (lower thick lines) and $n = 10^{-2}\mathrm{cm}^{-3}$ (upper thick lines). The upper panels show the results for $10^{-3}Z_{\odot}$ and those for the solar metallicity are shown in the lower panels. In the photoionization calculations the extragalactic ionizing spectrum without any modulation – HM model, (see Figure 1) at $z = 3$ (Madau & Haardt 2009) is assumed.

Figure 3 also shows the collisional time-dependent CIII fraction obtained using our code (thick solid line) and that taken from Gnat & Sternberg (2007) (thin solid line), as well as the CIE fractions obtained from CLOUDY (thin dash line). Firstly, one notes the difference of our results from the Gnat & Sternberg (2007) data. This difference can be explained by the fact that we use a different set of atomic data (radiative and dielectronic recombination rates) for several ions. We use the data for radiative recombination from Verner & Ferland (1996), which partially included the refitted data from previous works (see above for full list of papers), and for dielectronic recombination from Mazzotta et al. (1998). Gnat & Sternberg (2007) used more recent data of Badnell and coauthors (see references in Gnat & Sternberg 2007; Bryans et al. 2006). However, our CIE results are close to those obtained in CLOUDY code, which traditionally includes the most recent

atomic data[1]. So we assume that such difference may be mainly explained by small changes in thermal evolution. For example, it is well known that the dielectronic recombination depends exponentially on temperature, so we expect that for higher temperature and lower metallicity this difference becomes smaller (see Figure 3).

Secondly, we should note that both equilibrium and time-dependent collisional ionic composition has no dependence on gas density, because all processes are two-body. In contrast, the ionic composition in the photoionization case strongly depends on gas density. Moreover, the ionizing radiation forces the ionic composition of gas to settle on to equilibrium. In low density gas the ionic composition in the time-dependent photoionization case is expected to differ strongly from that in collisional both equilibrium and time-dependent cases, but it tends to the ionic fractions in the photoequilibrium. In high density gas we expect that the time-dependent photoionization ionic composition tends to the time-dependent collisional one, whereas the photoequilibrium ionic fractions should be close to those in the CIE. In addition, the ionic composition strongly depends on metallicity. For low metallicity the difference between time-dependent and equilibrium ionic fractions is expected to be small, but it increases with metallicity.

In Figure 3 one can see that the CIII fraction in the time-dependent photoionization model does not fully coincide in the whole temperature range with either the photoionization equilibrium or pure collisional models. For example, at low metallicity, $Z = 10^{-3}\ Z_{\odot}$, for high density value, $n = 10^{-2}$ cm^{-3}, the time-dependent photoionization CIII fraction shows some difference from the photo equilibrium case. In contrast, for $n = 10^{-4}$ cm^{-3}, the CIII fractions in the time-dependent photoionization and photo-equilibrium cases are close to each other in the whole temperature range. For solar metallicity, the difference between time-dependent and equilibrium photoionization becomes more significant for both number

[1]http://wiki.nublado.org/wiki/RevisionHistory

density values. Also one should note from the right panels of Figure 3 there is almost no dependence on metallicity in equilibrium photoionization case. The difference between the CIII fraction for 10^{-3} $Z_{\odot}$ and solar metallicities is only in the value of temperature reached in the cooling process: for higher cooling rate (solar metallicity) this temperature is lower.

As it is expected for higher density value, $n = 10^{-2}\mathrm{cm}^{-3}$, the CIII photoionization fractions are close to the collisional ones in both equilibrium and time-dependent cases in a wide temperature range. For example, the ionic fractions in time-dependent collisional (thick solid line) and time-dependent photoionization cases (thick dotted line) almost coincide for $\log T \gtrsim 4.7$ at $Z = 10^{-3} Z_{\odot}$ and for $\log T \gtrsim 4.18$ at solar metallicity. In summary, both time-dependent collisional and photoequilibrium in the presence of a significant ionizing radiation flux like the extragalactic background models produce the ionic composition, which differs from that in time-dependent photoionization model. Due to the very non-linear dependence of ionic fractions on temperature, metallicity and density it is difficult to say where it is possible to use time-dependent collisional or photoequilibrium models, so in the present work we use the more complex, but more adequate time-dependent photoionization model.

2.3. Dependence on the initial temperature

Here we should consider a choice of the initial temperature and ionic composition for our study of absorbers at the redshift range $z = 2 - 3$. Many cosmological simulations (Davé et al. 2001; Cen & Fang 2006; Bertone et al. 2008) show that the intergalactic gas at $z = 2 - 3$ mainly resides in the diffuse phase with a typical temperature $T \lesssim 10^5$K and overdensity $\delta < 1000$, and a small part of gas (in the best model this fraction is less than 5%, see e.g. Davé et al. 2001) can be found in the warm-hot phase with $10^5\mathrm{K} \lesssim T \lesssim 10^7\mathrm{K}$. It is expected that a gas enriched by metals and expelled from galaxies would have passed

through strong shock waves. Since the typical velocity of galactic winds varies from several tens to hundreds km s^{-1}, the intergalactic gas enriched by metals is likely to go through such shock waves. We assume that such a gas was initially heated by shocks up to the temperature $T \gg 10^4$K. We are interested in subsequent evolution of this shock-heated gas. Here also we should note, firstly, that the heating rate produced by the strong ionizing background at $z = 2 - 3$ does not allow low-density gas with $n \sim 10^{-4}\mathrm{cm}^{-3}$ to cool effectively below $T \sim 3.5 \times 10^4$K, and secondly, that here we do not include adiabatic cooling due to the expansion of the universe, which dominates over the radiative cooling for very low density gas, $n \sim 10^{-5}$ cm^{-3} at $z = 3$.

In the following set of calculations we study the dependence of the ionic composition evolution of a gas on the initial temperature T_i. We vary the initial temperature in a wide range $T_i = 5 \times 10^4 - 10^8$K. Here we follow the evolution of gas irrespective of the time needed to cool from T_i to the temperature value, when our stopping criterion (mentioned above) is reached. Further we compare the cooling time with the comoving Hubble time at $z = 2 - 3$. The gas cooling is strongly determined by both initial conditions of the gas (density, metallicity and temperature) and the UV background radiation. We assume the initial ionic composition corresponds to $T_0 = 2 \times 10^4$K. Taking such conditions we simulate a gas parcel with $T_0 = 2 \times 10^4$K that initially passes through a strong shock wave front with $T_s \gg T_0$. Because of the short ionization timescale of metals (ionization fraction of hydrogen reaches almost unity for $T_0 = 2 \times 10^4$K in both CIE and time-dependent cases) the ionic composition of a gas passed through a shock front with temperature $T_s \gg T_0$ is expected to tend to that with $T_i = 10^8$K at $T \lesssim T_s$. Certainly, if the initial temperature is low enough, then the ionic composition should strongly depend on the initial temperature value.

Figure 4 presents the CIII fraction (*upper* panels) and the CIII/CIV ratio (*lower*

panels) for different starting temperature values and the ionization composition initially corresponding to that in the CIE at $T_0 = 2 \times 10^4$K. In the upper panels (the left is for $Z = 10^{-3} Z_\odot$, the right is for the solar metallicity) the significant deviations from the CIII fraction for the evolutionary track with $T_i = 10^8$K is found for $T < 10^6$K, whereas the CIII fraction for tracks with $T_i = 10^6$K and $T_i = 10^8$K almost coincides. The time needed for cooling a gas from $T_i \sim 10^6$K with $n \sim 10^{-4}$ cm^{-3} and $Z \sim 10^{-3} Z_\odot$ is comparable with the comoving Hubble time at $z = 2$ ($t_H(z = 2) \simeq 1.1 \times 10^{17}$ s). The cooling times from $T_i \sim 10^5$K is slightly shorter than the Hubble time at $z = 3$, but the CIII fraction strongly differs from that for $T_i = 10^6$K. But here we are interested in the ionic ratios, and not in column densities of individual ionic species.

In the *lower* panels of Figure 4 the CIII/CIV ratio demonstrates a weak dependence on the initial temperature. The ratio for $T_i = 4 \times 10^5$K almost coincides with that for higher temperature values. For the lowest temperature value, $T_i = 5 \times 10^4$K, considered in this set of calculations, the ionic ratio settles to the common trend almost at the same temperature $T \lesssim 5 \times 10^4$K for $n = 10^{-4}$ cm^{-3} (in this case at the beginning the photoheating is significant) and at $T \lesssim 3.2 \times 10^4$K for $n = 10^{-3}$ cm^{-3}. One can see the vertical parts of the CIII/CIV ratio tracks. However, the time needed for settling on the common trend (the time at the vertical part of the track) is significantly lower than the time needed for reaching the stopping criterion. For instance, for a gas with $n = 10^{-4}$ cm^{-3} and $Z = 10^{-3} Z_\odot$ such a timescale is about 2×10^{15}s in case of the initial temperature $T_i = 5 \times 10^4$K, whereas the time of the calculation before the stopping criterion reached is more than order greater, $\sim 5.2 \times 10^{16}$s$\simeq 0.7 t_H(z = 3)$. The timescales for higher density or metallicity are smaller. Thus, for $T \lesssim 4 \times 10^4$K (that is consistent with the line widths inferred by Agafonova et al. 2007) the CIII/CIV ratio in a gas with initial temperature $T_i \gtrsim 5 \times 10^4$K almost coincides with that for $T_i = 10^6 - 10^8$K, and the timescale of calculation needed for reaching our stopping criterion is smaller than the comoving Hubble time at $z = 2 - 3$. In light of this, we

can start our calculations from temperature $T = 10^6$ K and consider the obtained CIII/CIV ratio. We should emphasize that we are interested in the temperature range $T \lesssim 4 \times 10^4$K, where the ionic ratios for $T_i = 5 \times 10^4 - 10^8$K are very close (see lower panels of Figure 4), thus, our conclusions are almost independent on the initial temperature value, if this value is greater than 5×10^4K. Further analysis of the dependence of ionic composition on the initial conditions is out of scope of this paper and will be done elsewhere.

3. CIII/CIV ratio

In this section we study the influence of the extragalactic ionizing background with and without HeII absorption on CIII/CIV ratio. Nonequilibrium ionization states are calculated for ultraviolet (UV) spectra at redshifts $z = 1.87, 2.48, 2.65, 2.83, 3$ (all spectral data were kindly provided by F. Haardt) for three models presented in Madau & Haardt (2009), hereafter MH09 (the abbreviations of models are the same as in MH09): a) absorption in the HeII resonant lines was neglected – HM model, b) the sawtooth modulation was added – $HM + S$ model, where HeII/HI=35 in optically thin absorbers, and c) the model where the ratio HeII/HI were artificially increased to 250 – DR (delayed reionization) model (for details see MH09).

Note that the MH09 spectra differ from the Haardt & Madau (1996, 2001) spectra. First, MH09 spectra include quasar contribution only, and, second, in the UV background calculations a QSO luminosity function from Hopkins et al. (2007) is used, which produces a very steep decline of the ionizing flux at high redshifts. Figure 1 shows the far UV part of the MH09 spectra for $z = 2.48$.

The left panel of Figure 5 shows CIII/CIV ratios in the equilibrium calculation (using CLOUDY) for $Z = 10^{-3} Z_\odot$ (but there is no dependence on metallicity in the equilibrium,

see Section 2.2 and right panels of Figure 3). The two middle panels of Figure 5 shows CIII/CIV ratios in the nonequilibrium calculation (using our program for nonequilibrium calculation) for $Z = 10^{-3}Z_{\odot}$ and solar metallicities, correspodingly, for UV background spectrum at $z = 2.48$. The difference between models without (HM) and with ($HM + S$) the inclusion of the sawtooth modulation is small for the whole range of metallicities and densities. The ratios for the HM and $HM + S$ models differ from each other only by a factor of ~ 1.3 for low density at $T \lesssim 10^5$ K and they almost concide for $n = 10^{-2}\mathrm{cm}^{-3}$ or at $T \gtrsim 10^5$ K. In the DR model the ratio $N(\mathrm{CIII})/N(\mathrm{CIV})$ is greater than those in the HM and $HM + S$ models by a factor of ~ 10 at $T \lesssim 10^5$ K. This factor decreases with the increase of density and metallicity. For example, for $n = 10^{-2}\mathrm{cm}^{-3}$ a significant difference can be found only at $T \lesssim 6 \times 10^4$ K for $Z = 10^{-3}Z_{\odot}$ and $T \lesssim 2 \times 10^4$ K for solar metallicity.

For high density ($n \gtrsim 10^{-2}$ cm^{-3}), the ratio is close to that in the collisional limit at $T \gtrsim 5 \times 10^4$ K. One can therefore conclude that large sawtooth modulation as present in the DR model leads to higher abundances of CIII ions by a factor of 10–1.3 for gas density $n = 10^{-4} - 10^{-2}$ cm^{-3}, respectively. The increase of CIII and CIV abundances in the DR model arises from the decrease of CV and CVI abundances, because of lower ionization flux in the energy range $\sim 50 - 500$ eV in comparison with two other models, so the growth of the CIII abundance is higher than that of CIV making CIII/CIV ratio higher.

Our results firstly show that the ratio of CIII/CIV is not significantly changed by the sawtooth modulation of HeII, as supposed by Madau & Haardt (2009). Since the ionization threshold of CIII (47.9 eV) lies within the Lyβ absorption feature from HeII, and that of CIV lies well beyond the range where HeII resonant absorption changes the spectrum, it was expected that observations of the CIII/CIV ratio along with the theoretically calculated spectrum would be a good probe of the physical conditions in the IGM at $z \sim 3$. Our detailed calculations confirm the Madau & Haardt (2009) claim that the ionization rate of

CIII does not significantly differ between the "HM" and "HM+S" spectra, although the "DR" spectrum does make a difference. In other words, the CIII/CIV ratio is a good probe only for distinguishing between the extreme cases of "HM" or "DR", and not for probing the attenuation caused by standard abundances of HeII in the IGM.

4. Statistical analysis

Agafonova et al. (2007) give measurements of CIII and CIV column densities for 10 absorbers in the redshift range $2 \leq z \leq 3$. We use the ratio $R = N(\mathrm{CIII})/N(\mathrm{CIV})$ to constrain the ionizing radiation at far-UV range (Table 1).

For our analysis we consider three models of ionizing radiation, as discussed in the previous section, in the redshift range $2 < z < 3$, the metallicity in the range $Z = 10^{-3}$–1, the number density in the range $n = 10^{-4}$–10^{-2} cm^{-3}, and temperature $T \leq 4 \times 10^4$ K. This range of temperature is consistent with the line widths inferred by Agafonova et al. (2007).

The measured ratio R_{ob} depends on the parameters n, T, Z and the model of ionization. One expects the Z, n and T to vary appreciably from one absorber to another and therefore the usual χ^2 approach cannot be applied. Only the background ionizing flux can be assumed to vary slowly with redshift. In the light of these assumptions, we define, for each absorber, $\epsilon = |R_{\mathrm{th}} - R_{ob}|/|\Delta R|$, here R_{th} are the CIII/CIV ratios from our models, R_{ob} are the the observed values, and ΔR are the corresponding errors on these measurements (Table 1). For each absorber, we search the entire parameter space of T, n, Z, for a given model of ionizing radiation corresponding to the redshift of the absorber. For any absorber, a model is deemed acceptable if $\epsilon \leq \sqrt{5}$ (that corresponds to 5σ-level of the theoretical model).

Our results for the three models are shown in Tables 2–4. As seen from the tables, the models HM and $HM + S$ can fit well for 8 out the 10 data points of Agafonova et al.

(2007). However, the DR model is acceptable for only six out of the ten absorbers. One absorber is fit well by none of the models (absorber 4).

In Tables 2–4 we also show the results for the equilibrium models using CLOUDY (Figure 3). The results in the two cases have qualitative similarities, e.g. absorber 4 is ruled out by all models. However, there are also quantitative differences. Many of the absorbers ruled out by the nonequilibrium models are now allowed or vice versa. An interesting departure between the two results is that the DR model is ruled out for as many as 8 absorbers.

Next we briefly discuss how our results depend on the choice of n, T, and Z. The preferred range of temperature is generally $\gtrsim$ a few $\times 10^4$ K to obtain acceptable solutions for all the absorbers. We do not list the best fit values of metallicity in the tables as the metallicities in the entire range we considered are allowed. We also note that this is also expected if the CIII/CIV ratios were obtained from equilibrium ionization models. We note that the dependence on n is stronger; the value of n is greater than $10^{-3}\mathrm{cm}^{-3}$ for all the acceptable models, except for the DR model. This is in line with the fact that the absorbers have densities comparable to or larger than virialized haloes at $z \simeq 3$, as distinct from smaller column density Lyman-α clouds which are only mildly overdense. In the measurements Agafonova et al. (2007) found a significant HI column densities, $N(\mathrm{HI}) \sim 10^{16-17}\mathrm{cm}^{-2}$. Also in the majority of the absorbers they detected singly-ionized carbon and silicon: $N(\mathrm{CII}) \sim 10^{13}\mathrm{cm}^{-2}$, $N(\mathrm{SiII}) \sim 10^{12}\mathrm{cm}^{-2}$, whose ionization potentials are below 13.6 eV. But detection of singly-ionized or neutral (like C, O or Si) species depends on the filling factor of cold clouds in the ISM of absorber and therefore it is not guaranteed that such a cold cloud must appear along the line of sight.

Even though this evidence is not conclusive to rule out the DR model, it is probably an indication that this line of enquiry is likely to better constrain the background far-UV flux.

We note that in absorbing systems with $N(\mathrm{HI}) \geq 10^{16-17}$ cm^{-2}, the UV background radiation above 54 eV may be attenuated (Haardt & Madau 1996; McQuinn et al. 2009). That can lead to higher ionic ratio N(CIII)/N(CIV), e.g. for the absorber no. 10 (see Table 1), thus the absorber no. 10 may suffer from self-shielding. But it is unlikely that the UV flux is severely attenuated in the case of other absorbers, because in the extreme case of zero flux, the ionic ratio N(CIII)/N(CIV) is expected to be larger than ~ 20 for $T \leq 4 \times 10^4$K, according to Figure 5 (the thin dot-dashed line for the collisional limit), and all absorbers except no. 10 show a smaller ratio than this, suggesting that attenuation of UV flux is unlikely to be a major problem.

5. Discussions

Our results suggest that it is possible to explain the ionic ratio without resorting to additional attenuation of UV flux between 3 and 4 Ryd by continuum HeII absorption, or a HeII GP effect. Agafonova et al. (2007) used their data to reconstruct the far-UV background radiation spectrum, and claimed a value of $\tau_{GP}(\mathrm{HeII}) \sim 2.5$–3. This was compared with other direct observations of HeII GP absorption trough, at $z = 2.87$, with opacity $\tau_{GP}(\mathrm{HeII}) \sim 2.09 \pm 0.1$ (Reimers et al. 2005). It is difficult to disentangle the effects of absorption from a continuous IGM and an ensemble of clouds, as in the case of HI GP effect (see Becker et al. 2007), although McQuinn (2009) has argued that the case for HeII GP effect is stronger than this, owing to the low abundance of HeII compared to HI. In light of the difficulty of identifying true GP effect, our results of explaining the ionic ratios of CIII/CIV with standard attenuation from HeII absorption suggest that the observations of Agafonova et al. (2007) do not necessarily need a HeII GP effect, although it cannot be completely ruled out.

Our results also clearly show that it is difficult to select one model of far-UV flux from

the observed data. It is possible that the measured ratios are sensitive to the local conditions inside the cloud. It is also possible that the far-UV radiation field is inhomogeneous over the redshift of probe. Available data from He II measurements suggests that the Strömgren spheres corresponding to this species might just be merging at $z \simeq 3$ (Jakobsen et al. 1994; Smette et al. 2002). Numerical simulations by McQuinn et al. (2009) have also shown that the reionization of HeII remains patchy even at $z \sim 3$. Therefore, it is entirely conceivable that it is inhomogeneous reionization and not fluctuation in the density, metallicity and temperature that is responsible for the wide range of observed CIII/CIV ratios.

A bigger data set involving different ionic ratios is however needed to address some of these questions in detail, and confirm the patchiness of the HeII reionization process. Also, to put better constraints on the spectrum profile we need to study ionization structure of a cloud coupled with gas dynamics and radiation transfer. Radiation transfer effects would particularly affect large HI column density clouds, and change the predictions of ionic ratios in them, but these effects are outside the scope of the present paper. Furthermore, the predicted ionizing background depends on the spectrum and luminosity function of sources, and this introduces an additional uncertainty in analysis of the kind we have presented here. It is possible that the effect of these uncertainties would be mitigated by studying different ionic ratios, and we will report the advantages of using other ions in a future paper.

6. Conclusions

In this paper we used the data of Agafonova et al. (2007) for abundance ratio of CIII to CIV in quasar absorption systems at $z \sim 2.4$–2.9, to constrain the spectrum of the cosmic UV background radiation. We have used the spectrum calculated by Madau & Haardt (2009) which took into account the modulation from HeII Lyman series lines, and also models which assume a large abundance of HeII by artificially increasing the HeII/HI ratio.

Our results can be summarized as follows:

1. The ratio between CIII/CIV is not a sensitive probe of the attenuation of the far-UV spectrum between 3 and 4 Ryd for standard abundance of HeII in the IGM.

2. The observed data do not favor the models with additional abundance of HeII in the IGM (the "DR", delayed reionization models).

3. There is a large variation in the fitted values of density and temperature for the absorption systems. This is indicative of an inhomogeneous reionization of HeII at these epochs, that has been suggested from numerical simulations, and our results lend support to these models.

Francesco Haardt is acknowledged for providing the UV background spectrum data and necessary explanations. Gary Ferland and CLOUDY community are acknowledged for creating of the excellent tool for study of the photo-ionized plasma – CLOUDY code. EOV is grateful to Yuri Shchekinov for his help and many useful discussions. This work is supported by Indo-Russian project (RFBR grant 08-02-91321, DST-India grant INT-RFBR-P-10). EOV is supported by the RFBR (project codes 09-02-00933, 09-02-90726 and 10-02-90705), by the Federal Agency of Education (project code RNP 2.1.1/1937) and by the Federal Agency of Science and Innovations (project 02.740.11.0247).

REFERENCES

Agafonova, I. I., Levshakov, S. A., Reimers, D., Fechner, C., Tytler, D., Simcoe, R. A., & Songaila, A. 2007, A&A, 461, 893

Arnaud M. & Raymond J., 1992, ApJ, 398, 394

Arnaud M. & Rothenflug R., 1985, A&AS, 60, 425

Asplund, M., Grevesse, N., & Sauval, A. J. 2005, in ASP Conf. Ser. 336, Cosmic Abundances as Records of Stellar Evolution and Nucleosynthesis, ed. T. G. Barnes III & F. N. Bash (San Francisco: ASP), 25

Becker, G. D., Rauch, M., & Sargent, W. L. W. 2007, ApJ, 662, 72

Bernardi, M. et al. . 2003, AJ, 125, 32

Bertone S., Schaye J., Dolag K., 2008, SSRev., 134, 295

Brown P. N., Byrne G. D., & Hindmarsh A. C., 1989, SIAM J. Sci. Stat. Comput., 10, 1038

Bryans P., Badnell N. R., Gorczyca T. W., Laming J. M., Mitthumsiri W., Savin D. W., 2006, ApJS, 167, 343

Cen R. & Fang T., 2006, ApJ, 650, 573,

Davé R., Cen R., Ostriker J.P., et al. , 2001, ApJ, 552, 473

Drake J. J. & Testa P., 2005, Nature, 436, 525

Ferland G. J., Korista K. T., Verner D. A., Ferguson J. W., Kingdon J. B. & Verner E. M. 1998, PASP, 110, 761

Gnat O. & Sternberg A., 2007, ApJS, 168, 213

Gnat O. & Sternberg A., 2009, ApJ, 693, 1514

Haardt F. & Madau P., 1996, ApJ, 461, 20

Haardt F. & Madau P., 2001, in Clusters of Galaxies and the High Redshift Universe Observed in X-rays, ed. D. M. Neumann & J. T. V. Tran

Hopkins P. F., Richards G. T. & Hernquist L., 2007, ApJ, 654, 731

Jakobsen, P., Boksenberg, A., Deharveng, J. M., Greenfield, P., Jedrzejewski, R., & Paresce, F. 1994, Nature, 370, 35

Kaastra J.S. & Mewe R., 1993, A& AS, 97, 443

Kingdon J. B. & Ferland G. J., 1996, ApJS, 106, 205

Madau P. & Haardt F., 2009, ApJL, 693, 100

Madau, P., & Meiksin, A. 1994, ApJ, 433, L53

Mazzotta P., Mazzitelli G., Colafrancesco S. & Vittorio N., 1998, A& AS, 133, 403

McQuinn, M. 2009, ApJ, 704, L89

McQuinn, M., Lidz, A., Zaldarriaga, M., Hernquist, L., Hopkins, P. F., Dutta, S., & Faucher-Giguère, C.-A. 2009, ApJ, 694, 842

Pequignot, D., Petitjean, P., & Boisson, C. 1991, A&A, 251, 680

Reimers D., Fechner C., Hagen H.-J., Jakobsen P., Tytler D., Kirkman D., 2005, A&A, 442, 63

Ricotti, M., Gnedin, N. Y. & Shull, J. M. 2000, ApJ, 534, 41

Schaye, J., Theuns, T., Rauch, M., Efstathiou, G., & Sargent, W. L. W. 2000, MNRAS, 318, 817

Shull J. M. & van Steenberg M., 1982, ApJS, 48, 95

Smette, A., Heap, S. R.., Williger, G. M., Tripp, T. M., Jenkins, E. B., & Songaila, A. 2002, ApJ, 564, 542

Sokasian, A., Abel, T., & Hernquist, L. 2002, MNRAS, 332, 601

Theuns, T., Bernardi, M., Frieman, J., Hewett, P., Schaye, J., Sheth, R. K., & Subbarao, M. 2002, ApJ, 574, L111

Vasiliev E.O., 2010, in preparation

Verner D. A., & Ferland G. J., 1996, ApJS, 103, 467

Verner D. A., Ferland G. J., Korista K. T. & Yakovlev D.G., 1996, ApJ, 465, 487

Verner D. A., & Yakovlev D.G., 1995, A& AS, 109, 125

Voronov G. S., 1997, At. Data Nucl. Data Tables, 65, 1

This manuscript was prepared with the AAS LaTeX macros v5.2.

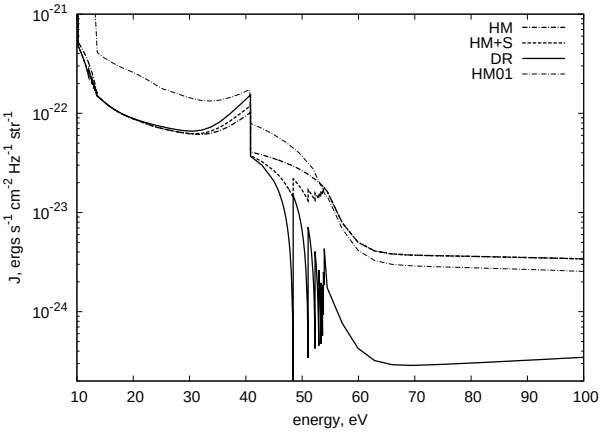

Fig. 1.— The far ultraviolet part of the extragalactic ionizing spectra at $z = 3$ (Madau & Haardt 2009): the spectrum without absorption in the HeII resonant lines – HM model – thick dot-dashed line, the spectrum with the sawtooth modulation – $HM + S$ model (HeII/HI=35 in optically thin absorbers) – thick dashed line, and the spectrum model where the ratio HeII/HI were artificially increased to 250 – DR (delayed reionization) model – thick solid line. For comparison the Haardt & Madau (1996, 2001) spectrum ($HM01$) for quasar-only (thin dot-dashed line) is added.

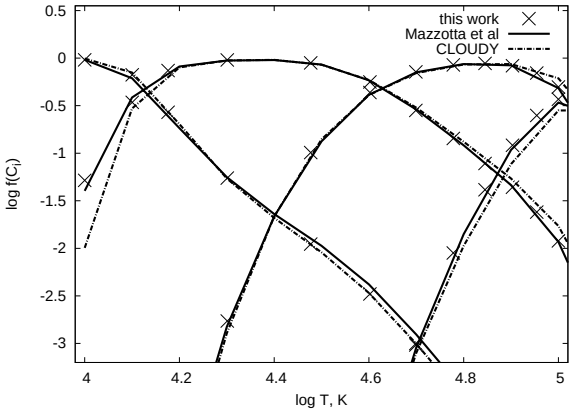

Fig. 2.— The collisional equilibrium carbon I-IV state fractions for our code (crosses) are superposed on the original results by Mazzotta et al. (1998) (solid lines) and the standard collisional equilibrium test of CLOUDY (dash-dotted lines).

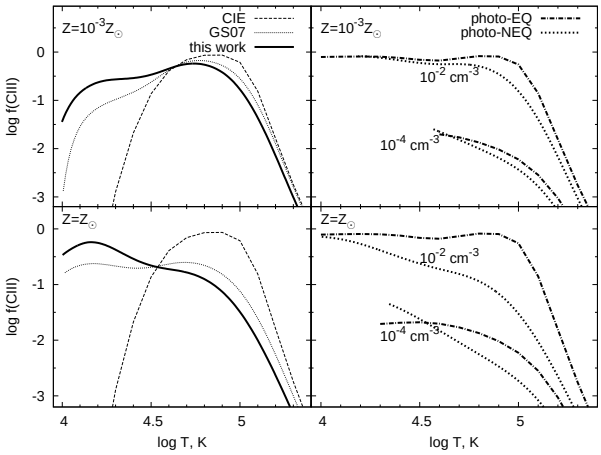

Fig. 3.— The CIII ion fraction for $10^{-3}Z_{\odot}$ (upper panels) and solar (lower panels) metallicities for collisional (left panels) and photoionization (right panels) cases. The collisional time-dependent ion fraction obtained using our code is shown by thick solid line and that taken from Gnat & Sternberg (2007) is depicted by thin solid line (GS07). In both left panels the CIE fraction of CIII obtained from CLOUDY is shown by thin dashed line. The time-dependent photoionization (thick dot lines, "photo-NEQ") and photo equilibrium (thick dash-dot lines, "photo-EQ") fractions are shown for $n = 10^{-4}$ cm^{-3} by lower thick lines and for $n = 10^{-2}$ cm^{-3} by upper thick lines, correspondingly. In the photoionization calculations the extragalactic ionizing spectrum without any modulation (HM model in Figure 1) at $z = 3$ (Madau & Haardt 2009) is assumed.

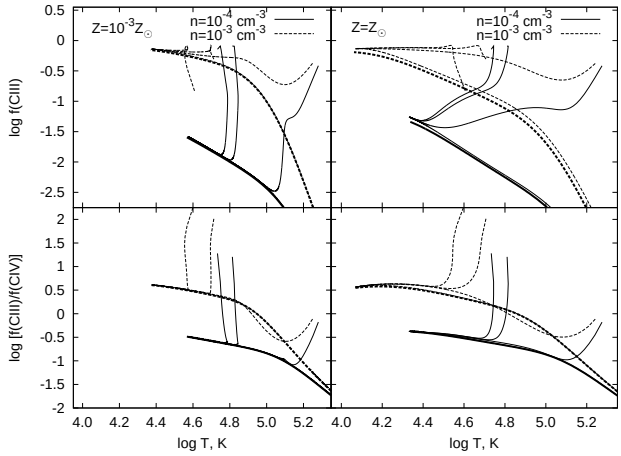

Fig. 4.— *Upper panels.* The CIII ion fraction for gas with $Z = 10^{-3}Z_{\odot}$ (left panel) and with solar metallicity (right panel), and $n = 10^{-4}$ cm^{-3} (solid lines), $n = 10^{-3}$ cm^{-3} (dashed lines) for different initial temperature values. Thick lines correspond to the initial temperature $T = 10^8$K, thin lines present the evolutionary tracks for initial temperature $T = 5 \times 10^4, 10^5, 4 \times 10^5, 10^6$K (from top/left to bottom/right). *Lower panels.* The CIII/CIV ratio for gas with the same parameters as in the *upper* panels.

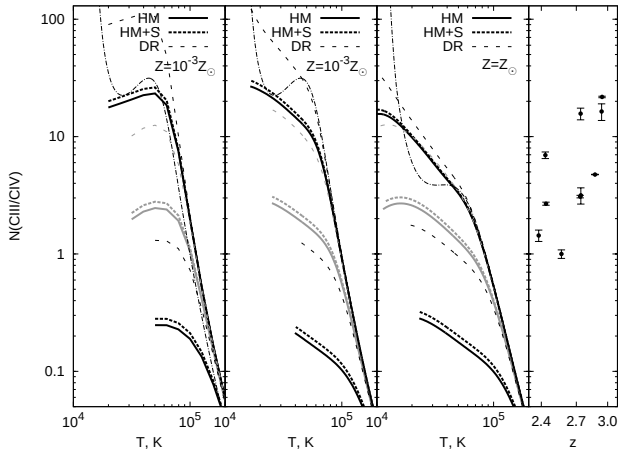

Fig. 5.— *Left panel.* The equilibrium CIII/CIV ratio for the Madau & Haardt (2009) spectrum at $z = 2.48$ for $Z = 10^{-3} Z_{\odot}$ metallicity is plotted as a function of gas temperature for various cases. The solid lines depict the ratio for the "HM" extragalactic spectrum, dashed lines – "HM+S", and dotted lines – "DR" models for three values of number density $n = 10^{-4}$, 10^{-3}, 10^{-2} cm^{-3} (from bottom to top). For clarity, the models with $n = 10^{-3}$ cm^{-3} are shown by gray lines. Thin dot-dash line corresponds to the ratio in the collisional limit: for $Z = 10^{-3} Z_{\odot}$. *Left middle panel.* The same as in the *left* panel, but for nonequilibrum models. *Right middle panel.* The same as in the *left middle* panel, but for solar metallicity. *Right panel.* The observational data of CIII and CIV column densities for 10 absorbers in the redshift range $2 \leq z \leq 3$ as given by Agafonova et al. (2007).

Table 1. Carbon ionization ratios for absorption systems

absorber	z_{abs}	$R = N_{\rm CIII}/N_{\rm CIV}$	error in R
1	2.379	1.438	0.160
2	2.433	6.944	0.449
3	2.438	2.680	0.082
4	2.568	1.000	0.083
5	2.735	3.083	0.076
6	2.739	15.681	1.782
7	2.741	3.158	0.499
8	2.875	4.750	0.025
9	2.939	16.363	2.645
10	2.944	21.765	0.311

Table 2. The best parameters for the model HM. Columns 2–4 present results for the nonequilibrium model. The next three columns show the results for the equilibrium model

absorber	T (K)	n (cm^{-3})	ϵ	T (K)	n (cm^{-3})	ϵ
1	40000	0.001	4	31622	0.001	2.1
2	27200	0.01	0.1	39810	0.001	8.2
3	30300	0.001	0.073	31622	0.001	1.82
4	21740	0.0001	6.9	31622	0.001	9.2
5	35460	0.001	0.02	39810	0.001	2.5
6	33300	0.01	0.027	19952	0.01	0.18
7	36370	0.001	0.005	39810	0.001	0.24
8	37920	0.01	1.36	39810	0.001	58
9	12840	0.01	0.006	25118	0.01	0.2
10	31730	0.01	0.15	25118	0.01	1.5

Table 3. Same as Table 2 for the model HM+S

absorber	T (K)	n (cm^{-3})	ϵ	T (K)	n (cm^{-3})	ϵ
1	39870	0.001	5.7	31622	0.001	2.83
2	28210	0.01	0.12	39810	0.001	6.68
3	34930	0.001	0.07	25118	0.001	0.85
4	23800	0.0001	6.1	31622	0.001	10.7
5	30200	0.001	0.1	39810	0.001	2.29
6	36310	0.01	0.04	19952	0.01	0.4
7	29410	0.001	0.02	39810	0.001	0.37
8	23400	0.001	0.4	39180	0.001	31
9	13670	0.01	0.032	19552	0.01	0.012
10	37070	0.01	0.015	39810	0.01	0.12

Table 4. Same at Table 2 for the model DR

absorber	T (K)	n (cm^{-3})	ϵ	T (K)	n (cm^{-3})	ϵ
1	39810	0.0001	0.24	31622	0.001	42
2	31100	0.001	0.02	31622	0.001	3.1
3	16840	0.0001	3.8	31622	0.001	68
4	39810	0.0001	5.7	31622	0.001	87
5	16840	0.0001	9.4	31622	0.001	68
6	37830	0.001	0.01	39810	0.001	0.14
7	16840	0.0001	1.6	31622	0.001	10
8	39990	0.001	10.8	31622	0.001	142
9	16710	0.01	0.001	39810	0.001	0.16
10	39630	0.01	0.015	39810	0.001	18